Model-Based Control of a High-Performance Marine Vessel

A Thesis

Presented to the

Graduate Faculty of the

University of Louisiana at Lafayette

In Partial Fulfillment of the

Requirements for the Degree

Master of Science

Nicholas Paul Bergeron

Fall 2014

Model-Based Control of a High-Performance Marine Vessel

Nicholas P. Bergeron

APPROVED:

Joshua Vaughan, Chair Assistant Professor of Mechanical Engineering	Mostafa Elsayed Professor of Mechanical Engineering
Arun Lakhotia Professor of Computer Science	Mary Farmer-Kaiser Interim Dean of the Graduate School

Acknowledgments

I would like to thank my advisor, Dr. Joshua Vaughan, for his great support and help. His encouragement and guidance have made me a better researcher and student. I would also like to thank my committee members, Dr. Mostafa Elsayed and Dr. Arun Lakhotia, for being a part of this process. I would like to thank Swiftships, Inc. and the employees there for assisting with the Anaconda project.

I would like to thank my fiancee, Trisha, for being by my side all the time and always lifting me up when I'm down. Her unending love and encouragement makes me the happiest I have ever been.

I would like to thank my parents, Bradley and Laurie, for always pushing me to be my best. Without their love and support, I would not be where I am today. I would like to thank my sister, Kasey, and all of my family for always being there for me.

Lastly, I would like to thank God for truly giving me everything I have and always being a beacon of light for my future.

Table of Contents

List of Tables

List of Figures

1 Introduction

For decades, autonomous navigation has been a desired goal. Slowly, small steps towards autonomous vehicles have been accomplished. For example, some sailboats have auto-tillers, which keep the sailboat on course even after wind changes [9]. However, in the recent past, larger steps towards autonomous navigation have been made. There are now semiautonomous drones, like the one in Figure 1, that patrol the skies of conflict areas and even some advanced cars that can drive themselves, like the one shown in Figure 2 [10, 11].

An area that could hold enormous potential in autonomous navigation is in the realm of water. With over 70% of the Earth's surface covered in water, vehicles that can successfully navigate the seas and inshore waterways present new applications for unmanned vehicles [12, 13]. The use of autonomous navigation in marine applications can hold high potential for civilian, military, industrial, and environmental applications. Environmental research could use robotic vessels that are able to constantly collect qualitative data and position information as they move through a study area. Industrial or civilian ships possessing the ability to move independently through high traffic areas and avoid accidents or collisions would be a valuable asset for any modern society. Military science is also seeking advances in this field that would allow autonomous boats to patrol borders and combat zones without risking human life.

Figure 1: Autonomous Predator Drone [2]

Figure 2: Google Self-Driving Car [3]

Unmanned vehicles in maritime applications hold many advantages over the use of crewed vessels. Navigation through inshore and offshore waters poses many threats and dangers to human operators due to the highly dynamic conditions. These external effects make the control of autonomous vessels challenging. However, a robustly-designed autonomous navigation system can eliminate human error in unpredictable conditions while removing the human operator from the dangerous conditions. Autonomous ships could become a viable option for navigating open seas and larger bodies of water [14, 15], eliminating the need for human physical presence on long voyages. Unmanned boats may also hold the key to highly precise navigation and improved performance in vehicle movements during nautical transportation [16].

With regard to military applications, unmanned maritime vehicles could be used for ensuring security within harbors, sweeping an area for mines, and securing critical waterways. The United States Department of Defense has expressed its desire for unmanned maritime systems because of these three driving forces: department budgetary challenges, evolving security requirements, and a changing military environment [17]. In the years to come, the military will increase the demand for unmanned maritime vehicles. These vehicles will allow a vastly larger portfolio of missions to be performed and a wider territory to be covered than manned vehicles.

Unmanned surface vehicles designed for civilian and industrial usage present a subset of unique problems that must be faced. Ships used to transport cargo and passengers generally must travel through high traffic ports, navigation canals, and shipping lanes. Maritime rules and regulations are in place to manage these travel corridors. Applying these maritime rules and regulations to autonomous marine vessels can be a challenge, but research has been done in this area. For example, Benjamin and Curcio created a convention of collision avoidance that abided by the Coast Guard Collision Regulations [18, 19]. This convention was applied to simulations and physical models to prove their effectiveness.

Due to the enormous potential in marine autonomous navigation, numerous controls systems have been developed to enable accurate control. Autonomous navigation controls must not only have the ability to reach a waypoint, but must identify obstacles, follow legal travel lanes, and follow regulations of marine travel, such as the International Regulations for Preventing Collisions at Sea [18, 19]. Most available research on autonomous navigation in watercraft focuses on platforms that are only capable of relatively slow motion [20–22]. Few applications of unmanned control have applied the technology to a high-performance vehicle [23, 24]. Autonomous controllers applied to a fast traveling craft must adapt rapidly due to the increased rate at which the vessel will approach target waypoints and obstacles that must be avoided [25]. Most systems consist of a form of adaptive feedback control or a basic proportional-intergral-derivative (PID) controller handling the error between a desired heading and the actual heading [14, 26, 27]. This method is fine for basic controls, but it presents a problem when high accuracy is needed due to environmental constraints. Model-based controllers are based on the vessel's dynamics allowing it to achieve high accuracy. This high accuracy makes model-based controllers the preferred type.

Model-based designs are valuable in the fact that they rely on accurate dynamic models to predict the behavior of the vehicle. Model-based controllers have been designed for other applications such as underwater gliders, autonomous helicopters, and autonomous rovers [21, 28, 29]. Some work, mostly theoretical, has been done using model-based controllers for marine applications [30, 31]. The most prevalent is the work done on dynamic positioning

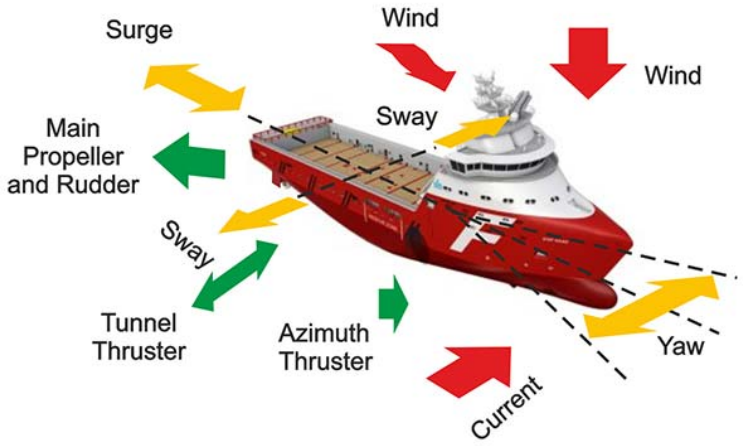

Figure 3: Forces Acting on a Ship Equipped with Dynamic Positioning [4]

for large vessels in open seas [31, 32].

The goal of dynamic positioning is to maintain a ship's position and heading. Dynamic positioning takes into effect all outside disturbances by using sensors to record the disturbances and incorporating them into a model of the vessel. An example of all the external forces acting on a ship equipped with dynamic positioning is shown in Figure 3. There are forces supplied by the boat that corrects any change in heading that may occur due to the external forces. For example, if the ship is at a desired location and the current, as shown in Figure 3, provides a sway to the ship, then the dynamic positioning system would engage the tunnel thruster to counteract this force. The tunnel thrusters would continue exerting force until the ship was back in its desired location. Any external force may push the ship off course, but the ship is equipped with a tunnel thruster, azimuth thruster, and main propeller and rudder to adjust and counteract any external forces that may displace the ship from its desired location.

The dynamic positioning system is used often in the oil and gas industry to maintain a position over a fixed point at the bottom of the waterway or to maintain a relative speed to another moving ship [33]. However, small vessels have had little physical model-based control work applied to them; most research has focused on the area of large ships [34, 35]. The work that was done on small vessels did not include vessels with high-performance capabilities and high maneuverability [14, 15, 36]. This presents the opportunity to create a

model and controller specific to a small high-performance marine vessel.

1.1 Previous Work

Some of the work on larger vessels that pertain to model-based control systems has been relatively extensive. Fossen created a unified model that combined a low frequency model and a wave frequency model [34]. The low frequency model was created using the assumption of calm seas with respect to ship maneuvering, station-keeping, and control in a seaway. Then, a wave frequency model that was dependent on the state of the sea besides calm seas was created. Then, these two models were superimposed on each other to create a unified model that can be used to simulate ships in a seaway. This model applies to rudder and propellor driven large vessels. Before this recent work had been accomplished, PID controllers were commonly used to control the autopilots of ships [37]. This autopilot relied on a reference model of the ship that took in as inputs the desired heading as well as a feedforward control based on the wind. With these inputs and using the PID controller and reference model, the corrected course heading was calculated. In the field of dynamic positioning, the ships originally used three decoupled PID controllers to control the horizontal motion of ships. These original PID controllers were not based on a model of the ship, and, therefore, disturbances that entered the feedback loop had provided complications. Balchen eventually applied linear quadratic optimal controllers and the Kalman filters to this problem [31, 38]. This motivated the use of model-based control systems on ships using dynamic positioning to give the process a higher accuracy.

In smaller vessels, most research done in relation to model-based control systems has been on vessels with low performance capabilities or a comprehensive study was not done. Vaneck created a fuzzy guidance controller for waypoint following on a 1.4 m long and 23 kg vessel [14]. A dead reckoning algorithm was used for the controller to calculate the desired heading and distance to the next waypoint. This technique was done without creating a mathematical model of the vessel's dynamics, which allowed rapid design but had to be tuned before final implementation. Dhariwal and Sukhatme used a modified radio controlled airboat to create a controller for waypoint following [36]. A dynamic model was created of the boat and using sensors and this model, a controller was developed and

was based on follow-the-carrot/goal method. Using the current location estimate, the controller computes the distance to the next waypoint and desired heading. Using these computations, a PID controller then generates the commands for the boat. Model-based control has been done before in small and large vessels; however, it has not been done for a high performance small vessel that will be demonstrated later.

In this thesis, a highly maneuverable vessel built by Swiftships, Inc. based in Morgan City, Louisiana will be used. This marine vessel, shown in Figure 4, is called the Anaconda and is a special operation craft riverine (SOCR) [5]. The Anaconda is 35 feet (10.7 meters) long and is designed to operate in shallow or confined waterways such as rivers. It is made from aluminum and is propelled by a twin water jet propulsion system giving it a max speed of 50+ knots (25.7 m/s). This jet propulsion system allows for turning by adjusting the angle of the nozzles from the rear of the vessels. A capability of the Anaconda that attributes greatly to its maneuverability is a bucket system located directly behind each nozzle. A picture of this bucket and nozzle system is shown in Figure 5. As seen in the figure, the bucket can be lowered by hydraulic rams to cover the nozzle and divert the jet stream.

Figure 6 shows the location of the water jet assembly in comparison to the full Anaconda. These buckets allow the user to direct the thrust towards the rear of the boat giving for-

Figure 4: Swiftships' Anaconda [5]

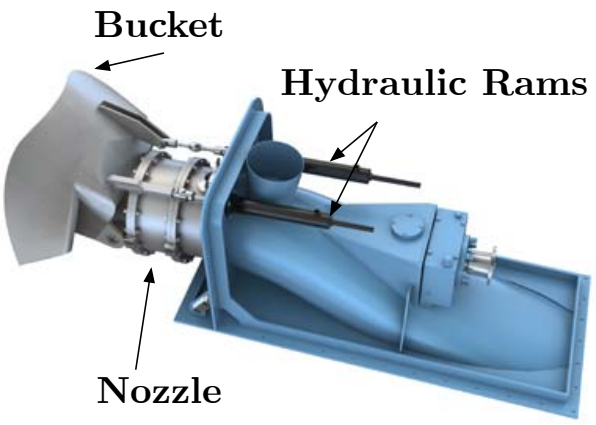

Figure 5: Bucket and Nozzle System [6]

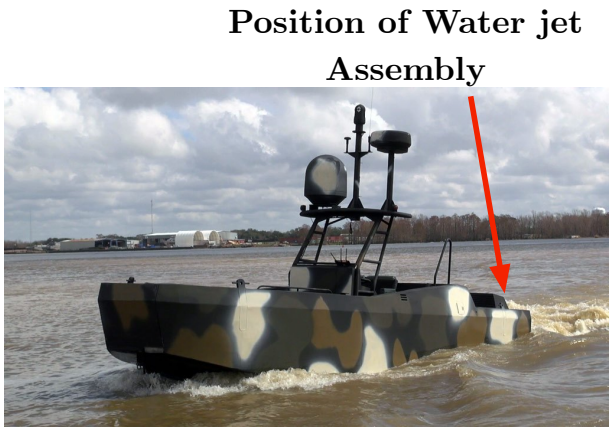

Figure 6: Location of Water Jet Assembly [7]

ward propulsion, direct the thrust towards the front of the boat giving rear propulsion, or any variation in between. Each bucket can be controlled independently, which gives the vessel the capability of tight turns by employing the buckets, as well as changing the direction of the nozzles.

1.2 Thesis Contributions

This thesis makes significant contributions to the understanding of the dynamics and model-based control of a highly-maneuverable marine vessel. The main contributions are:

1. A dynamic model of a highly-maneuverable marine vessel.
2. A model-based controller for a highly-maneuverable marine vessel that provides basic autonomous capabilities.
3. A remote control allowing for communication between the marine vessel and the user via a graphical user interface.

These contributions are significant because there has not been an extensive survey of the dynamics and the use of those dynamics to form a model-based controller on a marine vessel with this maneuverability. The bucket-and-nozzle system on the Anaconda provides a platform that has extreme capabilities and although this technology is not new, the comprehensive study that was done on it is.

1.3 Thesis Outline

Chapter II focuses on the modeling of the marine vessel. It presents the basic model of the marine vessel, then performs the tests for finding the parameters of the marine vessel. Using these parameters, an accurate model is created and compared to other tests. Chapter III focuses on the controller based on the model obtained in Chapter II. It demonstrates the validity of the controller based on comparison to experimental data. The advances in autonomous navigation of the marine vessel are discussed. The hardware and setup that allowed autonomous and remote control navigation will be demonstrated followed by future work and concluding remarks.

2 Modeling and Simulation

This chapter presents more detail about the Anaconda and the resulting dynamics of it. The derivation of a model for the Anaconda is discussed, and results from the simulations that were designed specific to the Anaconda are shown. Experimental tests run on the Anaconda support the validity of the derived model. A comparison of experimental results and simulations is also shown.

2.1 Anaconda

The vessel that will be used as a basis for tests and modeling is the Anaconda built by Swiftships, Inc. Swiftships, Inc. is a ship building company located in Morgan City, Louisiana. They specialize in aluminum and steel marine vessels and maintain contracts throughout the globe. The Anaconda is designed primarily for riverine conditions. However, it can remain fully operational in Sea State 2 conditions. The sea state conditions are shown in Table 1 [1]. This table shows that the average wave height that the Anaconda is designed for will be less than 1 foot with the wind only classified as a gentle breeze with a speed of 7-10 knots. Since Sea State 2 or below conditions are the Anaconda's operational range, then it can be seen that the magnitude of waves or wind will not be great enough to contribute significantly to the dynamic forces exerted on the Anaconda.

Table 1: Sea State Conditions [1]

Sea State	Description
Sea State 0-1	Sea glossy to small wavelets, crests do not break, Wind ranges 0-6 knots (calm to light breeze), Average wave height 0-0.18 feet
Sea State 2	Large wavelets, crests begin to break, glossy foam, Perhaps scattered white caps, wind ranges 7-10 knots (Gentle Breeze), Average wave height 0.6 feet
Sea State 3	Small waves, fairly frequent white caps, wind ranges 11-16 knots (moderate breeze), Average wave height varies from 1.4-2.9 feet depending on wind velocity.
Sea State 4	Moderate waves taking a more pronounced form, many white caps, chance of spray, wind 17-21 knots (fresh breeze), Average wave height 3.8-5.0 feet depending on wind velocity

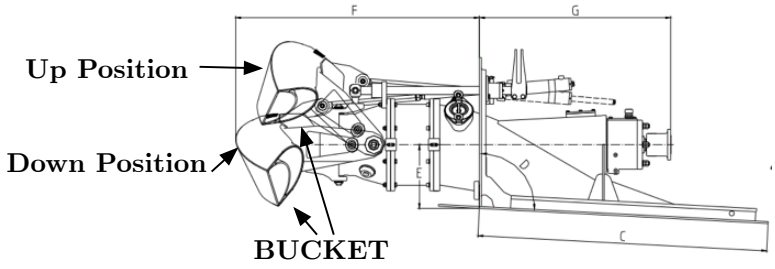

Figure 7: Bucket Design [8]

2.1.1 Specifications

The craft is 35 feet (10.7 meters) long with a beam of 8 feet (2.4 meters) and a draft of approximately 21 inches (53.3 centimeters) with a full load, therefore giving it the capability to operate in shallow waters. This vessel was built for use by special operations forces to deploy quickly and efficiently. It is powered by two Yanmar 1500 hp diesel engines, and propulsion is provided by two Rolls Royce FF-Series water jets. This propulsion system can provide speeds of over 50 knots (25.7 m/s). The exterior of the water jets is comprised of a bucket-and-nozzle system that provides steering and directional propulsion.

2.1.2 Anaconda Propulsion and Steering

The arrangement of the bucket-and-nozzle system allows for the adjustment of the multi-position buckets that alter the vector of thrust provided by the water jets as shown in Figure 7. By changing the position of the buckets, the direction of the jet streams exiting the nozzles changes.

This alters the direction of the water column produced by the jets. Nozzle steering, illustrated in Figure 8, occurs when the helm on the boat is turned. When the helm is turned to the port, the nozzles of the water jets will also turn port in relation to the position of the helm. With the nozzles turning port, they will focus the propulsion to the port side enabling the boat to turn in that direction. The nozzle-based steering is used most frequently for low-angular-velocity turning (*i.e.* "normal" conditions). It can be supplemented by the buckets to add increased turning agility.

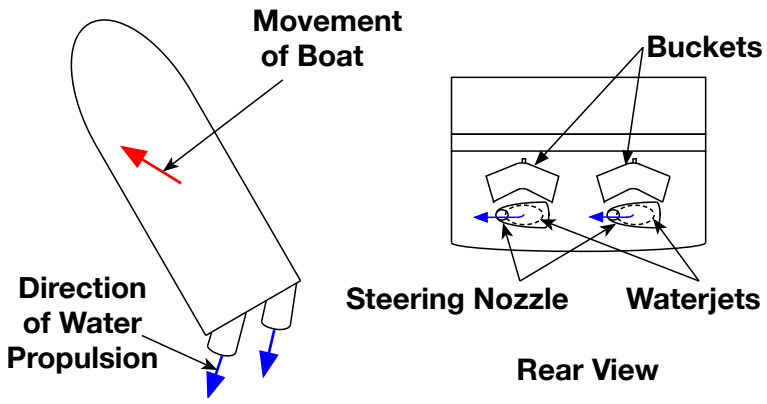

Figure 8: Nozzle Steering

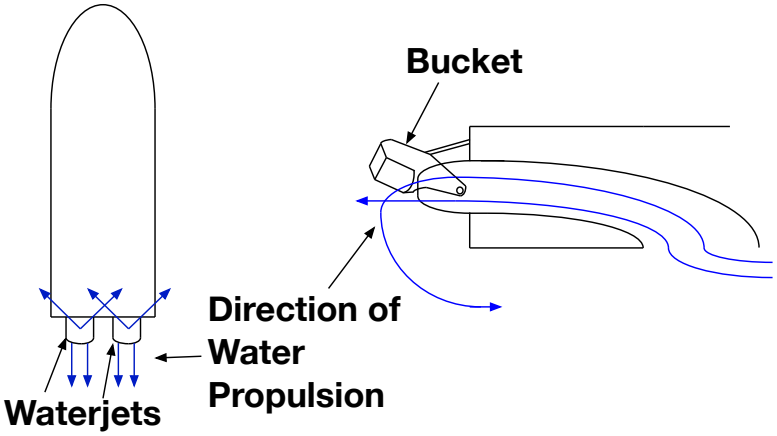

Figure 9: Neutral Thrust Bucket Position

The buckets are designed to allow for the redirection of the thrust. The curvature of the buckets allows them to redirect the thrust under the boat or provide uninterrupted thrust out its back. When the bucket is in the neutral position, as shown in Figure 9, the bucket is placed directly in front of the nozzle. This position allow half of the thrust to flow straight out the back while the other half diverts under the boat. These thrusts are equal and opposite, so the boat remains stationary.

When the buckets are in the full-up position, the water jet flowing from the nozzles is uninterrupted, resulting in forward motion. The full-up bucket position is shown in Figure 10. Opposite of this, when the buckets are in the full-down position, the thrust is fully directed underneath the marine vessel which propels the ship in full reverse, as shown in Figure 11.

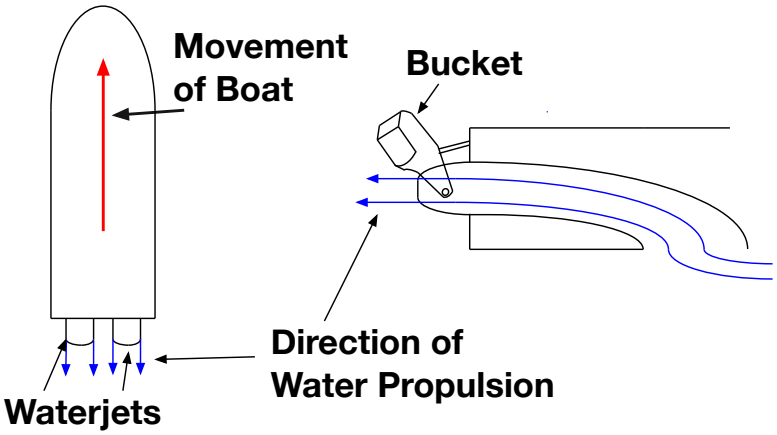

Figure 10: Forward Thrust Bucket Position

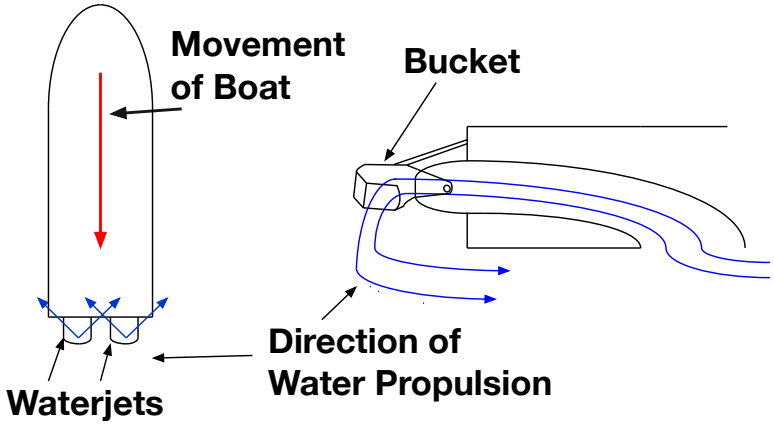

Figure 11: Reverse Thrust

The buckets are capable of any position in between full-up and full-down positions, and the port and starboard buckets can be controlled independently. With this independent bucket control, the vessel can be turned by using the buckets. Lowering the position of the bucket to the jet on the same side of the ship as the direction of the desired turn will allow the turn to be made. For example, if the ship is traveling in a full-forward heading, the bucket on the starboard jet would be engaged downward to perform a starboard turn, as shown in Figure 12. As seen in the figure, when the port side bucket is lowered, it reverses some of the port thrust underneath the boat. Since the starboard side bucket stayed in the raised position, the starboard thrust continued to expel out the rear uninterrupted. The causes a port turn due to the moment that these forces create.

Ships that use this type of water-jet system are able to perform some maneuvers that con-

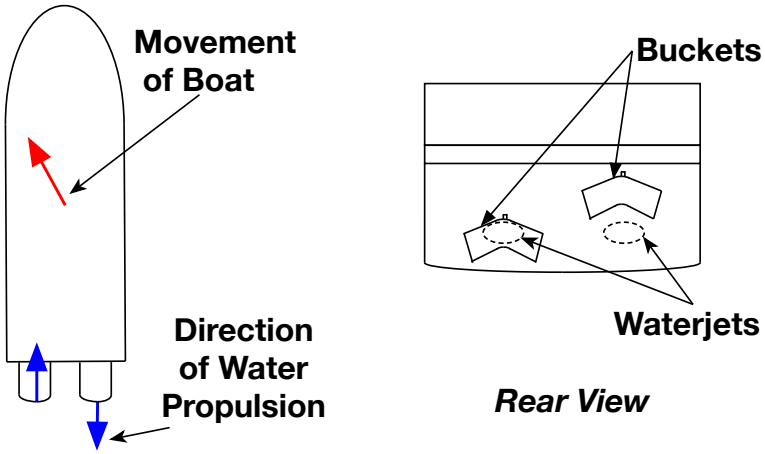

Figure 12: Turning with the Buckets

ventional propellor-driven and rudder-steered vessels cannot. For example, the operator can use the reverse positions of the buckets to perform an emergency stop from full speed. The operator of the Anaconda can also rapidly change the heading of the craft by altering the nozzle steering position and incorporating the buckets. All of these maneuvers can also be performed when the ship is at planing speeds.

The buckets are controlled separate of the helm using a series of control levers. There is one control lever for each of the bucket, which allows for independent control. Most operators of the vessel use the helm for steering while the bucket levers are used as a transmission to allow the boat to choose between forward, neutral, and reverse. This bucket-and-nozzle system allows for high performance and highly-maneuverable capabilities that large vessels do not possess and that is not common in smaller vessels.

2.2 Dynamics

Many studies have been done on dynamics on marine vessels since the basics amongst each vessel are similar [22, 35, 36]. However, the basics are not suitable to fully quantify the dynamics of a specific marine vessel. Most dynamic models propose 6 degrees of freedom as shown in Figure 13.

These six different motion components are defined as surge, sway, heave, roll, pitch, and

yaw. As shown in Figure 13, heave is the linear vertical (up/down) motion, sway is the linear lateral (side-to-side) motion, and surge is the linear longitudinal (front/back) motion. The rotational motions are defined as roll, pitch, and yaw. Pitch is the rotation of a vessel about its transverse axis. Roll is the rotation of the vessel about its longitudinal axis. Yaw is the rotation of a vessel about its vertical axis. The x-direction is defined as the axis that passes through the boat down the keel. The y-axis is defined as the axis that passes through the center of gravity of the boat across the beam of the vessel. The z axis is the vertical axis extending above and below the boat through its center of gravity. The variables representing the motions are predefined by standard maritime research.

In open seas, all 6 of these degrees of freedom must be accounted for. Heave, roll, and pitch are normally associated with the rocking of the boat due to external environmental factors. One of these main factors would be waves. Since this small vessel is mainly a riverine vessel and is operational in Sea State 2, the chances that it encounters significant waves are low. The assumption is made that heave, roll, and pitch are not dominant effects on this vessel. Based on this assumption, heave, roll, and pitch are disregarded and the only concern is with the remaining 3 degrees of freedom, surge, sway, and yaw acting in the X-Y-Z body-fixed frame. This simplified coordinate system is shown in Figure 14.

With the 3 degrees of freedom defined, the forces acting on the Anaconda are defined as shown in Figure 15. The current is the major environmental force that will be acting on the marine vessel. Figure 15 shows that depending on the direction of the current rela-

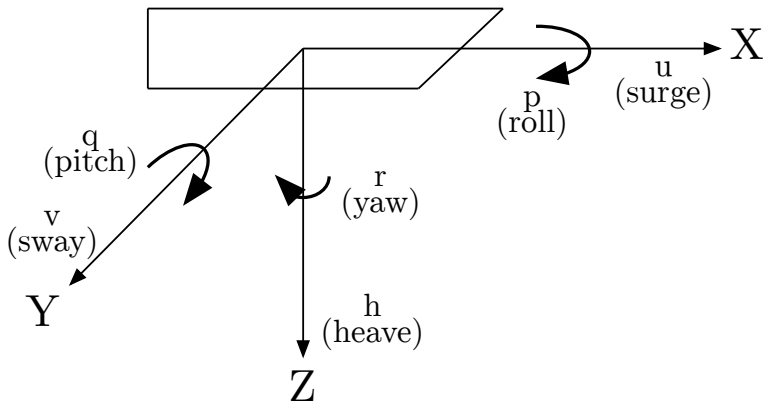

Figure 13: 6 Degrees of Freedom

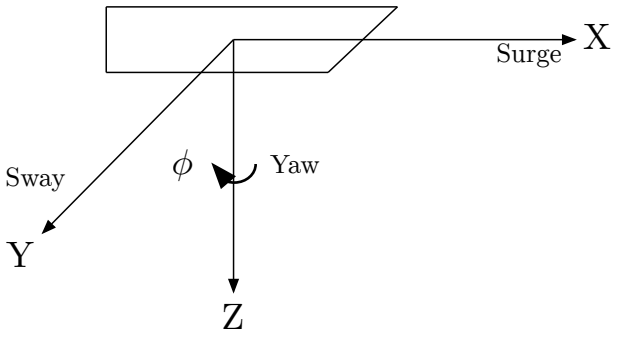

Figure 14: 3 Degrees of Freedom

tive to the heading of the vessel, the current could have forces in the X or Y direction. The figure also shows that with two water jets on the Anaconda, there are two propulsion forces acting on the rear of the vessel. The magnitude and direction of these propulsions can be changed by a combination of throttle percentage, bucket placement, and nozzle direction.

Anytime movement through a fluid occurs, there will be resistance to each direction of travel. With the Anaconda traveling through water, there are hydrodynamic forces acting on it in the opposite direction of travel. All of the forces acting on the Anaconda are the propulsion, hydrodynamic, and current forces. When taking all of these forces into consideration, the linear motion of the Anaconda is described by:

$$m\ddot{\bar{x}} = \bar{F}_{lprop} + \bar{F}_{rprop} + \bar{F}_h + \bar{F}_{cur} \tag{1}$$

In this equation, the coordinate system is fixed to the center of gravity of the vessel. $\bar{F}_{lprop}$ and $\bar{F}_{rprop}$ are the propulsion forces provided by the water jets. $\bar{F}_h$ is the hydrodynamic forces acting against the movement of the vessel, and $\bar{F}_{cur}$ is the force of the current. These are the two external forces that have dominant effects on the dynamics of the Anaconda. As shown in (2), $\bar{x}$ is the vector of generalized coordinates, x and y, therefore showing that (1) represents linear motion in the X and Y direction.

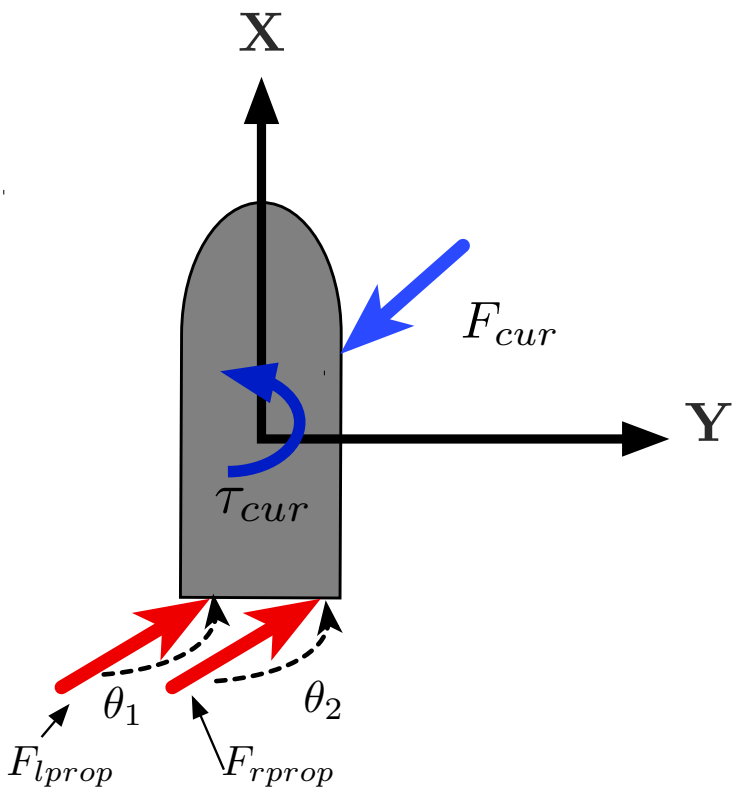

Figure 15: Current and Propulsion Forces

$$\bar{x} = \begin{vmatrix} x \\ y \end{vmatrix} \tag{2}$$

These same forces also affect the angular motion of the Anaconda. The resulting equation of motion defining the angular motion is:

$$I\ddot{\phi} = \bar{\tau}_{cur} + \bar{\tau}_h + [F_{lprop} \sin\theta_1]d + [F_{rprop} \sin\theta_2]d \tag{3}$$

In (3), $\bar{\tau}_{cur}$ is the torque created by the current, while $\bar{\tau}_h$ is the torque created by the hydrodynamic forces, and the d is the distance from the center of gravity of the Anaconda to the back of the boat where the propulsion forces are acting in the Y direction, as shown in Figure 16. In the figure, ϕ is the angle of heading, while θ_1 is the angle of F_{lprop} from the Y-axis and θ_2 is the angle of F_{rprop} from the Y-axis as shown in Figure 15.

While the Anaconda has the ability to control each of the nozzles individually during operation, in normal operation the nozzles move in tandem and therefore maintain the same angle. The assumption is made that the nozzles and throttles will move as one and can then be treated as a single force. Also, the two propulsion forces are assumed equal to each other because when the buckets are not being used, the forces are equal. The model is simplified based on this assumption and the resulting equation is:

$$I\ddot{\phi} = \bar{\tau}_{cur} + \bar{\tau}_h + 2[F_{prop}\sin\theta]d \tag{4}$$

The simplified model can be seen in Figure 17. The hydrodynamic forces account for the entire motion of the boat in all 3 degrees of freedom. There will be a hydrodynamic force affecting the yaw, surge, and sway whenever the boat has motion in these directions. The hydrodynamic forces in the body-fixed X direction are [35]:

$$\bar{F}_{hx} = m(\ddot{x} - \dot{y}\dot{\phi}) \tag{5}$$

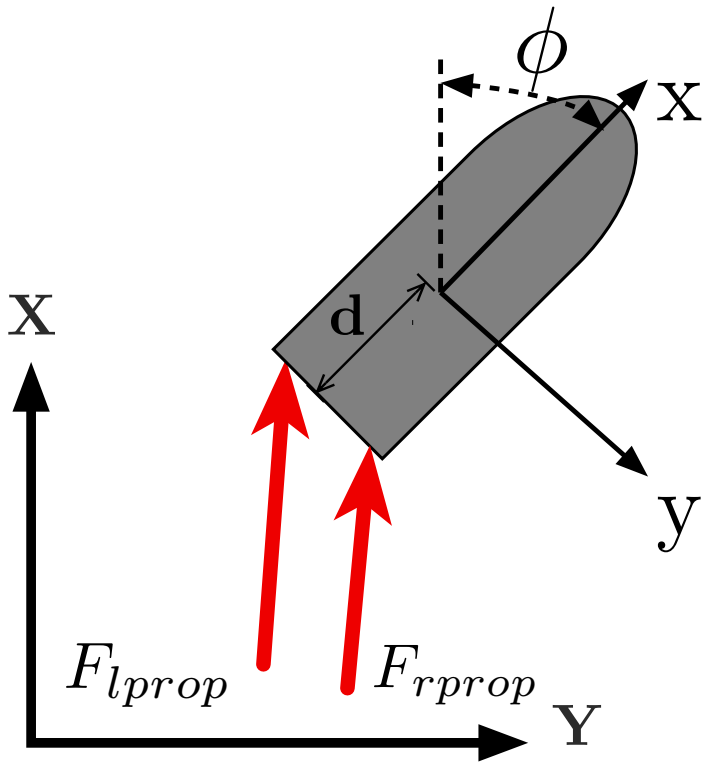

Figure 16: Model

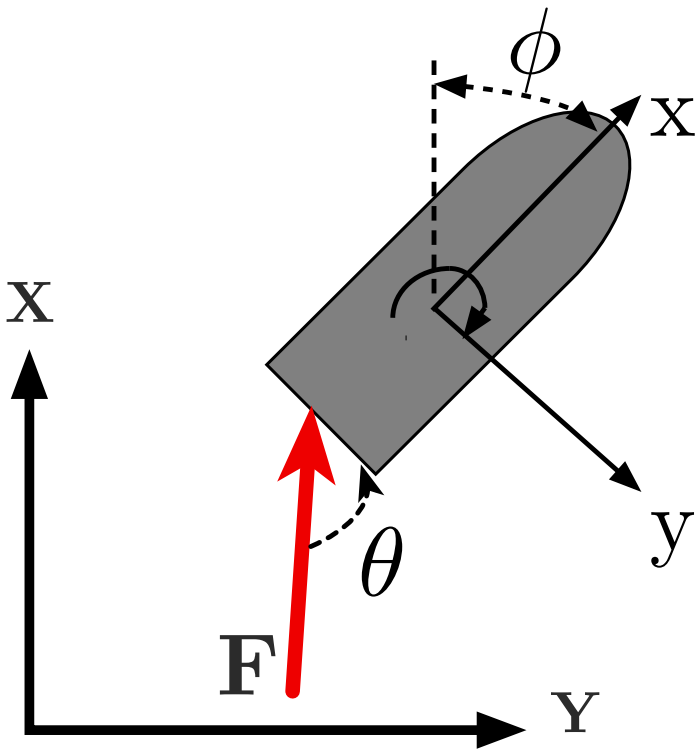

Figure 17: Simplified Model

The hydrodynamic forces in the body-fixed Y direction are [35]:

$$\bar{F}_{hy} = m(\ddot{y} - \dot{x}\dot{\phi}) \tag{6}$$

Finally, the hydrodynamic forces acting opposite of angular motion are [35]:

$$\tau_h = I_z\ddot{\phi} \tag{7}$$

Table 2 sums up the variables and their uses in the previous equations.

2.3 Modeling Using Simplified Model

The simplified model as shown in Figure 17 is used as the basis for the modeling. For simplification, some assumptions are made, which include restricting the propulsion forces from going in reverse as well as restricting them from going above a maximum. All tests are done on non-planing speeds with a maximum speed of 4 m/s. When achieving planing speeds, the vessel has enough power to pull itself out of the water and maintain a plane

Table 2: Nomenclature

Variable	Definition
ϕ	angle of heading
θ	angle of nozzle
$\vec{F}_{prop}$	force of propulsion
$\vec{F}_h$	hydrodynamic forces
$\vec{F}_{cur}$	force of current
$\vec{\tau}_{cur}$	torque due to current
$\vec{\tau}_h$	torque due to hydrodynamic forces

with the surface of the water. When this is accomplished, the boat sits higher out of the water and the boat becomes more stable on the water [39].

2.3.1 Fixed Point Path Following

An arbitrary end point was defined at coordinates (100 meters, 100 meters) for the boat to track towards using a Proportional-Derivative (PD) controller with a proportional gain, k_p, of 33 and derivative gain, k_d, of 1000. The block diagram showing the layout of the controller is shown in Figure 43. The PD controller is employed in a feedback system and compares the desired heading, ϕ_d with the current heading, ϕ. The gains were selected by gain tuning the simulation until stability occurred and oscillation had dissipated. The parameters in Table 3 were used for the models. The mass of the Anaconda was taken from the Swiftship's listing of the characteristics of the vessel. The moment of inertia, I_z was $1043m^4$. I_z was calculated using an approximation of the dimensions of the vessel. The maximum value of propulsion force, F_{max}, was calculated using experimental data showing the acceleration response of the vehicle, discussed later in Section 2.5.2.

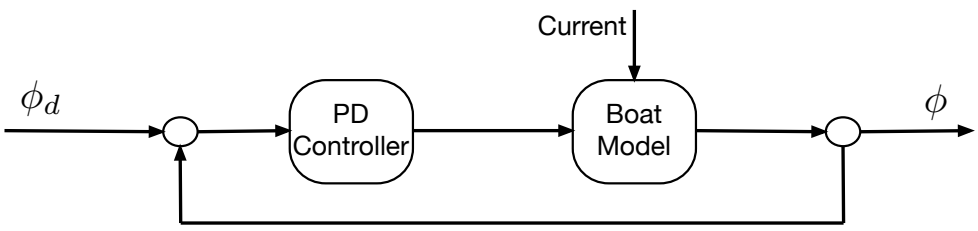

Figure 18: Block Diagram of PD Controller

Table 3: Parameters

Parameter	Value
m	11484 kg
I_z	1043 m^4
F_{max}	2296 N

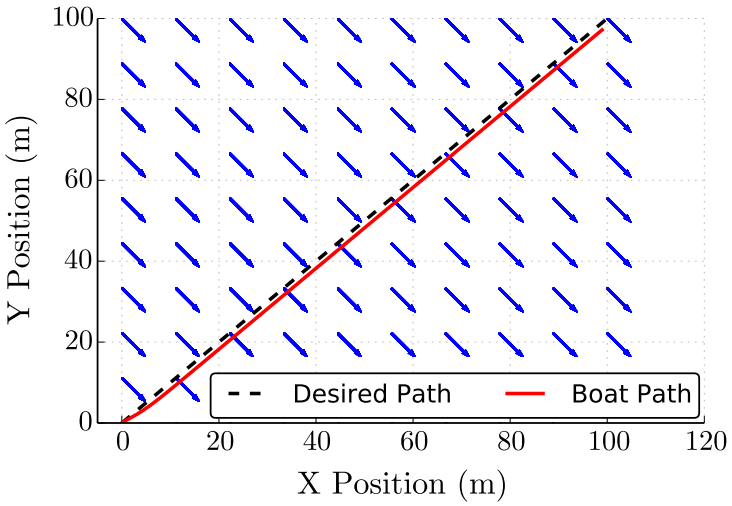

Figure 19: Path of Boat Going to a Desired Point

An example, a point-to-point move of the Anaconda is shown in Figure 19. The desired end point's coordinates are taken and divided by the trial time. This gives the fraction that must be moved each time step. This fraction is multiplied by the time step to give the desired x and y coordinate at each time step. This forms a trajectory which the PD controller measures against along the way. A non-derivative kick version of the PD controller is being used to calculate the forces required to reach the desired point at each time step. In Figure 19, the actual path taken versus the desired path as well as the direction of the current is also shown. In the figure, the boat deviates slightly away from the desired path due to the force of the current. The boat must then work its way back to the desired path as it nears the goal target.

Figures 20 and 21 show the differences between the desired location at that instant compared to the actual location. This desired location is not the goal point, but instead one of the many points located along the ideal travel course. The figures show that there was more of a difference in the Y direction. This is due to the fact that a larger part of the

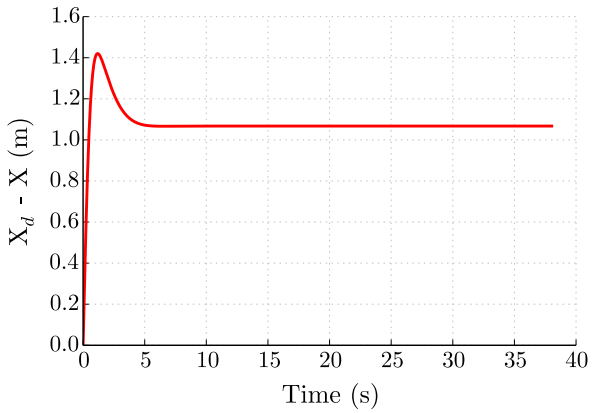

Figure 20: Difference Between X_d and X

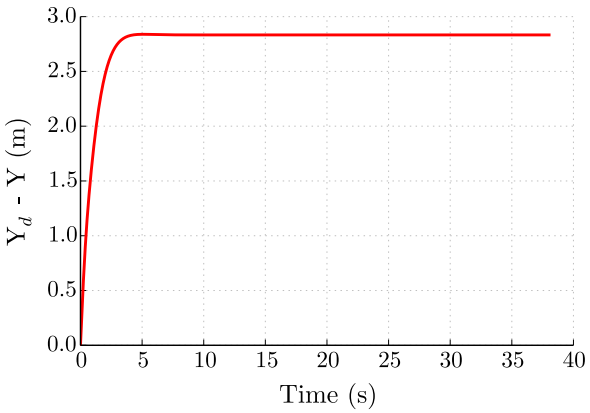

Figure 21: Difference Between Y_d and Y

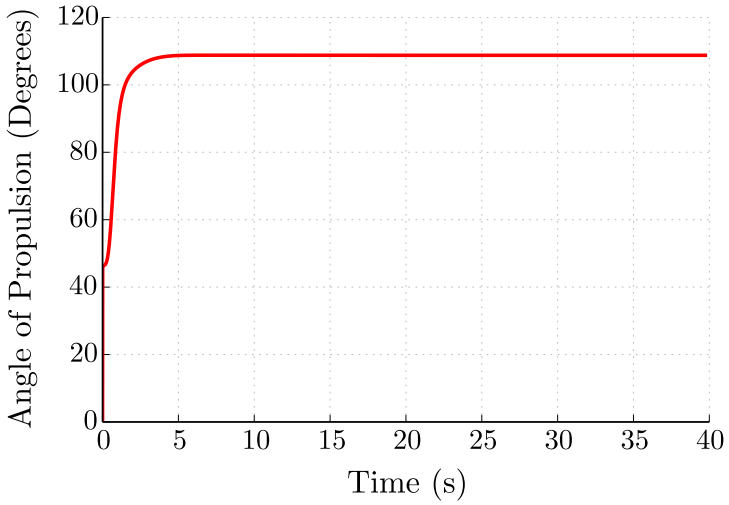

Figure 22: Angle of Propulsion

magnitude of the current was focused in the Y direction, therefore making the vessel have more external forces on that axis.

Figure 22 displays the angle of propulsion force exerted by the water jets. The water jets exhibit some overshoot in the beginning but then maintain a nearly constant angle to obtain a constant turning radius back to the desired path as shown in Figure 19. The reason for this constant positive angle of propulsion is due to the fact that the boat is constantly trying to negate the effects of the current.

Another point-to-point simulation was run with the desired point at (20 meters, 80 meters). The same gains were used as before: kp of 33 and kd of 1000. Figure 23 shows the

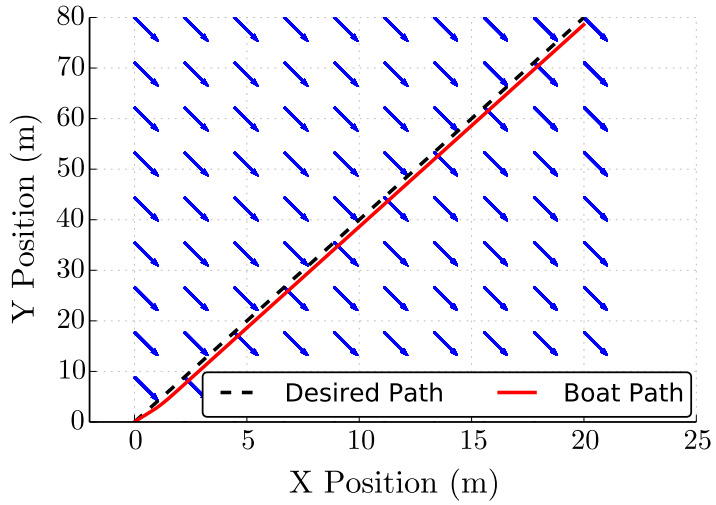

Figure 23: Path of Boat Going to a Desired Point

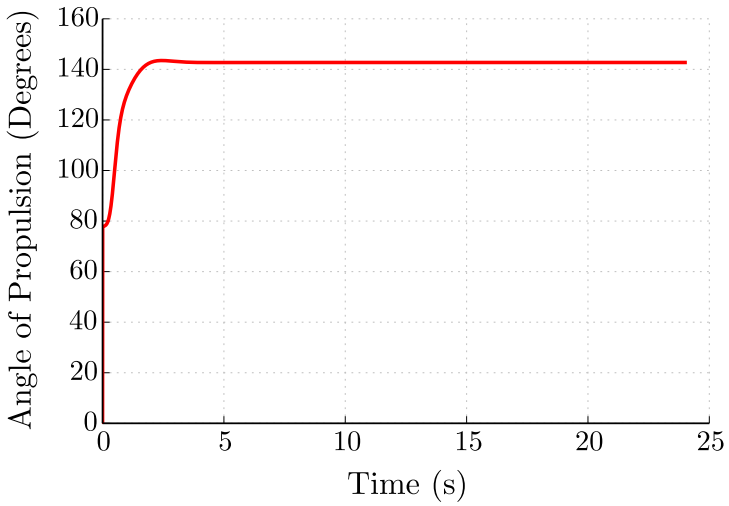

Figure 24: Angle of Propulsion

actual path taken versus the desired path taken. The external force of the current is acting on the vessel and therefore, preventing it from following the straight desired path.

Figure 24 shows the angle of propulsion sharply increase then level out to counteract the forces of the current. Figures 25 and 26 show the differences between the desired location at that instant compared to the actual location. As shown, the model has a higher error in the y direction since this is the direction that the majority of the magnitude of the current acts in.

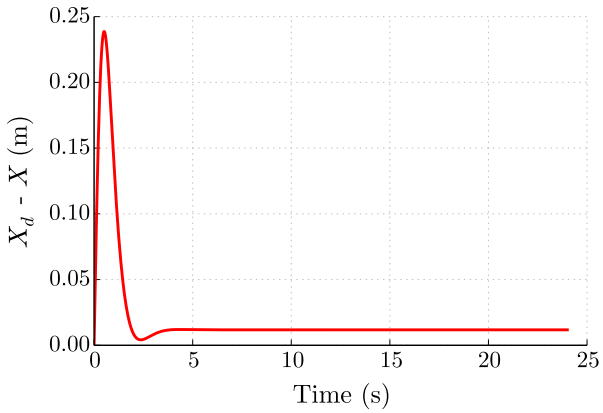

Figure 25: Difference Between X_d and X

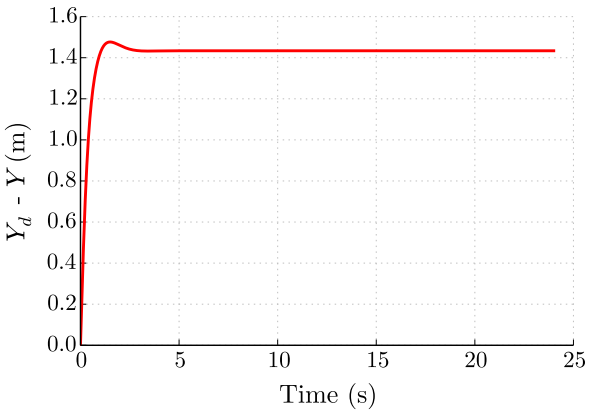

Figure 26: Difference Between Y_d and Y

2.4 Simplification of Boat Model and Simulated Transfer Function

To define the turning and acceleration response, the equations of motion were further simplified, and a transfer function for each of these responses was obtained. This simplification was obtained by making assumptions based on the simplified model in Figure 17 and the combination of the external and environmental forces. The hydrodynamic forces and current forces were combined since both of these forces are acting against the boat. Equation (8) shows the combination of the hydrodynamic forces and currents together as one resistance force proportional to the boat's velocity.

$$m\ddot{\bar{x}} = \bar{F}_{prop} + \bar{F}_{resistance} = \bar{F}_{prop} - c_1\dot{\bar{x}} \tag{8}$$

The simplified version of the original equation of motion representing the linear motion is:

$$m\ddot{\bar{x}} + c_1\dot{\bar{x}} = \bar{F}_{prop} \tag{9}$$

c_1 represents the damping effects of the hydrodynamic properties. Based on the simplified linear equation of motion, the input would be the F_{prop} which would influence an output of $\dot{x}$ or the velocity of the boat. Due to this, the input can be portrayed as the percentage of throttle applied, since the F_{prop} is determined by that, while the output is the velocity achieved by the boat.

$$\frac{sX}{F} = \frac{\frac{1}{m}}{s + c_1/m} \tag{10}$$

The resulting first order transfer function is:

$$\frac{\text{Boat Speed}}{\%\ \text{Throttle}} = \frac{K/m}{s + c_1/m} \tag{11}$$

where K is the gain that represents the scaling between the transfer function of this simulated transfer function and the experimental transfer function. Equation (11) shows the relationship between the throttle input and the resulting velocity.

The same method of simplification was used in the angular motion, as well. Along with treating the hydrodynamic and current forces as one resistance, the propulsion forces were combined and treated as one force from the rear of the vessel. Simplifying the hydrodynamic and current forces into one resistance force and taking the dual propulsion force as one, the equation of motion becomes:

$$I_z\ddot{\phi} = \bar{\tau}_{resistance} + \bar{F}_{prop} \sin\theta \tag{12}$$

Portraying the resistance force as a form of a damping effects and representing $\sin\theta$ with θ:

$$I_z\ddot{\phi} = \bar{F}(\theta) - c_2\dot{\phi} \tag{13}$$

The input will be the direction of the nozzles, θ, while the output will be the heading, ϕ. The transform function for the turning response is:

$$\frac{\text{Heading}}{\%\ \text{Turn}} = \frac{KF/I_z}{s\left(1 + (c_2/I_z)s\right)} \tag{14}$$

F is assumed constant, while $\frac{c_2}{I_z}$ are representative of the hydrodynamic forces. It is treated as a resistance force because that is what hydrodynamic forces are in the simplest form. The is important because as the vessel turns there will be hydrodynamic forces acting against it.

2.5 System Identification

During experimental trials, the dominant dynamics of the Anaconda were determined at non-planing speeds. The non-planing speeds were used because contract obligations prevented experiments from going above non-planing speeds. This maximum speed was maintained at 4 m/s for the experimental trials. To collect the data during the trials, GPS and an Inertial Measurement Unit (IMU) are used. The data from these sensors was used to obtain an acceleration and turning response of the Anaconda. For each run, a minimum of three trials was conducted at varying parameters within the set.

2.5.1 Turning Response

A set of tests was conducted at the allowable speeds to examine the turning dynamics. A range of frequencies are applied to turning commands allowing the boat's steering dynamics to be observed. The commands given to the Anaconda proceed from a full right turn to a full left turn. Figure 27 shows an example of the turning response to a sine-wave steering

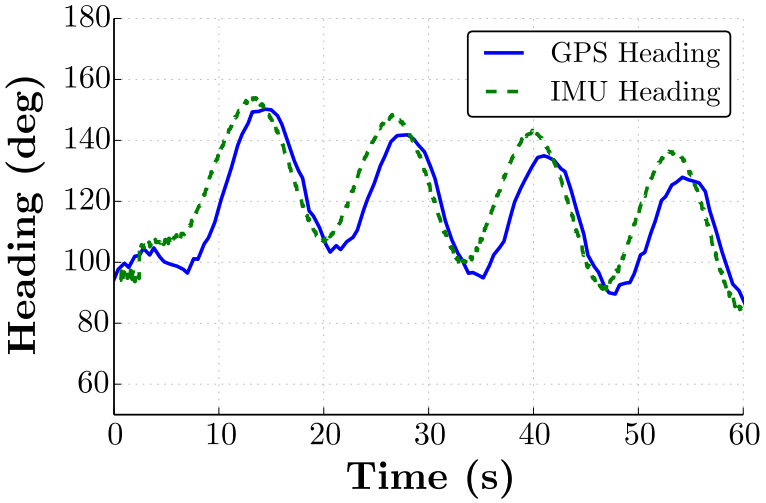

Figure 27: Example Turning Response Trials

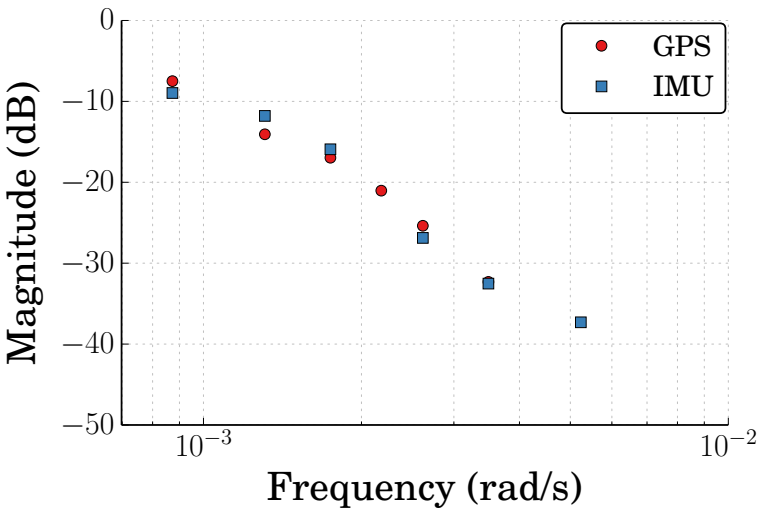

Figure 28: Experimental Turning Responses

input whose amplitude covered the entire range of steering angles. As shown in the figure, there are some inconsistencies between the GPS and IMU sensors which are due to the inaccuracies that are present on the sensors. Even with the inaccuracies, the data between the IMU and GPS data are in agreement.

After running multiple tests of different frequencies the results of the turning results were summarized into Figure 28. For each frequency that was tested, a set of IMU and GPS data was obtained. This data was then plotted on a bode plot to show the frequency response. Some tests had occurrences when the sensors did not prove credible or did not record accurate data. This result explains why some frequencies only have one type of sensor data. The data shown represents the average of the three trials at each turning frequency. As seen on the plot, there is strong agreement between the GPS and IMU data.

For steering, the first-order steering model by Nomoto is used [40]. The input from the control computer is the percentage of maximum steering angle, with -100% representing a full port turn and 100% representing a full starboard turn. The output is the heading of the vessel. The resulting transfer function is:

$$\frac{\text{Heading}}{\%\ \text{Turn}} = \frac{K_2}{s\,(1+\tau s)} \tag{15}$$

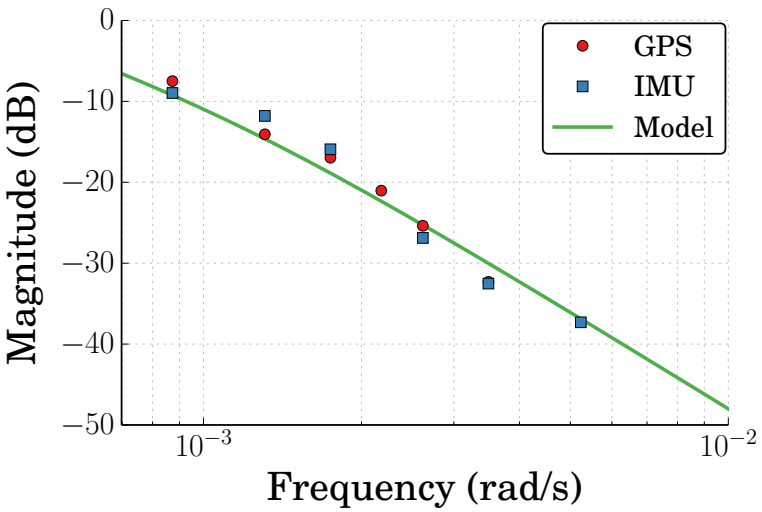

Figure 29: Comparison of Simulated and Experimental Turning Responses

whereas τ is representative of the hydrodynamic influences on the vessel. Figure 29 displays a model spanning the experimental turning responses. From this simulated model a transfer function for the turning response was created. The simulated results in Figure 29 provides a good match to the experimental data. With this comparison, the transfer function from (15) shows to be a good match to represent the yaw rate to the nozzle angle on the Anaconda.

2.5.2 Acceleration/Deceleration Response

Tests were performed to determine the acceleration and deceleration characteristics of the Anaconda. The tests were conducted by beginning at rest and was then given a full-throttle command. Full throttle was maintained for thirty seconds to allow the Anaconda to reach its maximum-allowable velocity. After thirty seconds, the throttles were reduced to zero. The trial ended when the boat returned to rest. An example acceleration response is shown in Figure 30. Both the raw GPS speed data and a filtered version of it are shown on the figure. As seen on the figure, the Anaconda achieved its maximum-allowable speed in approximately 10 seconds and maintained that speed for 20 seconds. After the 30 second mark, the throttle was reduced to zero and the next approximately 12 seconds saw the Anaconda's speed reduce by 75%.

During the experiment, the Anaconda achieved a maximum speed of approximately 4 m/s.

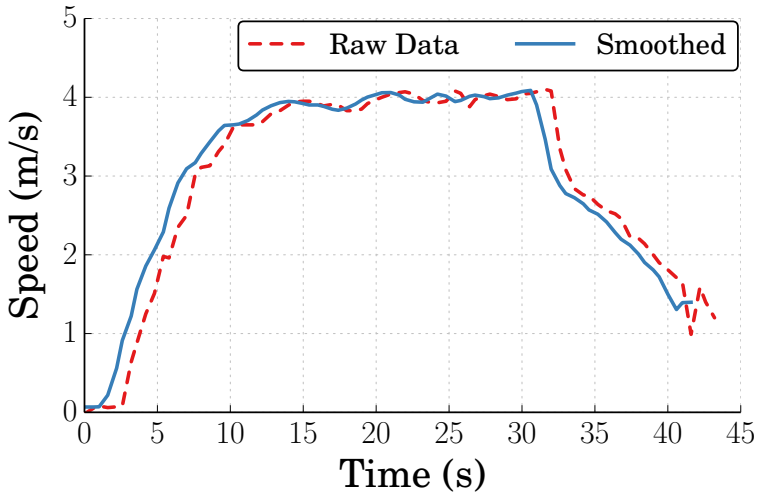

Figure 30: Example Acceleration Trial

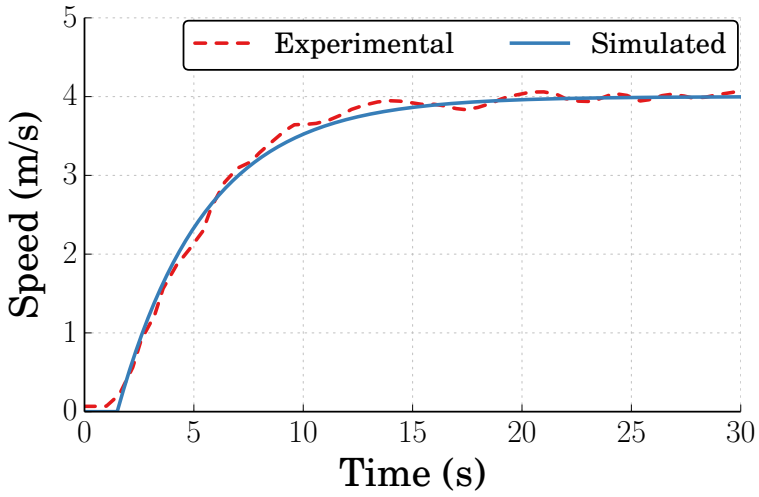

Figure 31: Comparison of Simulated and Experimental Acceleration

A first-order transfer function between the percentage throttle and the boat's speed was chosen to model the Anaconda's throttle response. This resulting transfer function is:

$$\frac{\text{Boat Speed}}{\%\ \text{Throttle}} = \frac{0.01}{s + 0.25} \tag{16}$$

Using (16) to create a simulated acceleration response and comparing to the experimental results, Figure 31 was created. It compares this first-order model of the Anaconda's acceleration dynamics to the experimental response. There is good agreement between

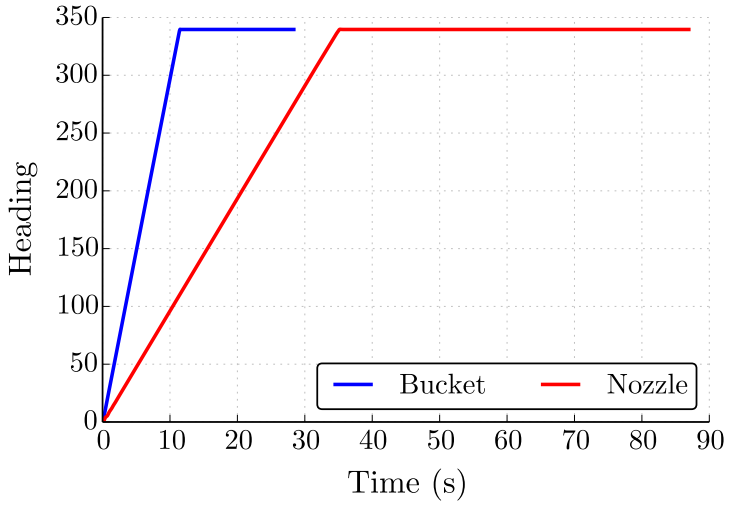

Figure 32: 340-degree Turn Using Nozzle Steering

the simulated and experimental results. When comparing (16), the experimental transfer function, to (11) there are similarities. They are both a first-order system. In comparison the numerator of the experimental transfer function was 0.01 while the numerator of the model-based transfer function was $\frac{K}{m}$. When equating these two numerators and using the mass in Table 3 the K equals 114.84. This is the scaling factor that must be taken into effect to relate the experimental and model-based transfer functions.

2.6 Modeling With Buckets

The coupled nozzle and bucket system is what makes the Anaconda very unique in the area of its performance capabilities. These models are navigating towards a desired heading ϕ. The error was calculated using the same PD controller as in Section 2.3. A model designed after the bucket capabilities was tested in comparison to a model with only nozzle steering incorporated. Figure 12 shows how the buckets operate to ensure a turn. When one bucket is placed over the nozzle and the other bucket remains in the up position, then the boat will make a turn towards the same side as the lowered bucket. While using the buckets, the Anaconda can make tighter turns then if just using nozzle steering alone. Figure 32 shows a turn of 340 degree turn of the model while using only nozzle steering. As can be seen in the figure, the model took approximately 35 seconds to complete the turn then it maintained that heading for the rest of the simulation.

The same procedure was done using the model that allows the buckets to do the turning instead of the nozzles. The bucket used in the turning was not pushed into the full down position; however, it was slightly lowered to allow a redirection of some of the thrust under the vessel. As seen in Figure 32, the heading change is much quicker when using the buckets. It only takes the vessel approximately 8 seconds to make the same turn. The time for a heading change when using the buckets is approximately one-third of the time it takes the nozzle system. This comparison exemplifies the performance capabilities that the Anaconda has and some of the maneuvers that it can accomplish.

2.7 Modeling Conclusion

In this chapter, the marine vessel that is being modeled was introduced. The dynamics of the Anaconda were derived and simplified down to a representative single propulsion force. These dynamics were applied to a mathematical model which allowed the behavior of the Anaconda under constant current conditions to be seen. The first example of this fixed point path following was done going to an end point of (100 meters, 100 meters). The vessel followed with a slight variation off of the desired path due to external forces. A second example was shown with a different end point with the same results. A simplified model and transfer functions were created from the assumption of both propulsion forces being equal to each other and all external forces were grouped together as a resistance. These transfer functions of the steering and acceleration response were compared to experimental transfer functions and shown to be in agreement with each other, thereby verifying the simplified model. In performing a turn with just nozzle steering and then bucket steering, it was validated that the buckets do provide better turning capabilities which makes the Anaconda unique in these capabilities. In conclusion, the assumptions that were made were proven accurate based on experimental data and the capabilities of the Anaconda's buckets were shown.

3 Controls

3.1 Heading Change

To determine the characteristics of the model-based controller, tests that compare the model-based controller and experimental data were run. These tests consist of changing to a desired heading from the current heading. On the experimental tests, IMU data was used to determine the current heading as well as track the difference between the desired and current heading. Figure 33 shows a 40 degree turn from an experimental test and model-based simulation. The experimental is not smooth due to the slight inaccuracies in the IMU as well as the environmental factors affecting the IMU. The model-based simulation was made to fit by changing the proportional gain, k_p, to 1500000 and the derivative gain, k_d, to 0.01. As seen in the figure, this provides an accurate fit to the experimental test.

Figure 34 demonstrates another test with only an 8 degree turn. The gains were kept the same as in the case before which provided a match to the experimental results. The figure also shows that there is no overshoot as well.

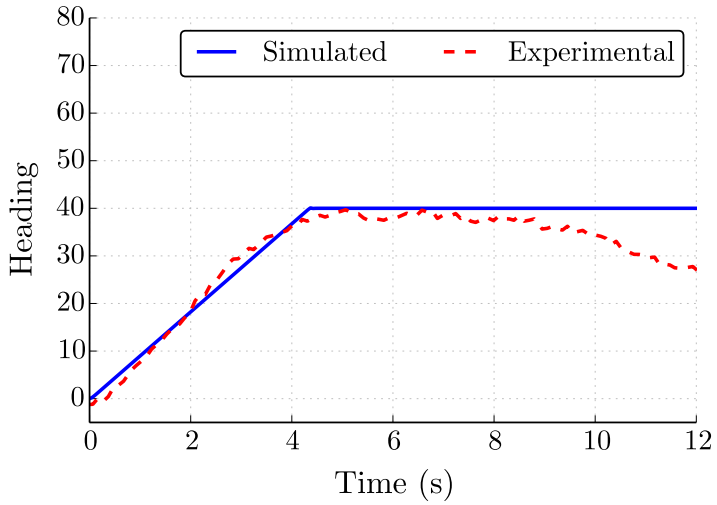

Figure 33: 40 Degree Turn

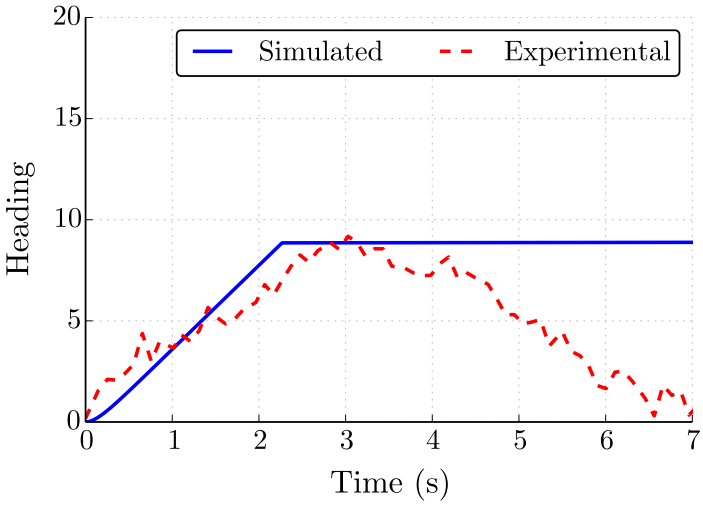

Figure 34: 8 Degree Turn

3.2 Autonomous Navigation

3.2.1 Point-to-Point Autonomous Navigation

A degree of autonomy was accomplished using the findings of the system identification. This autonomy was in the form of navigation to GPS coordinate waypoints. In these autonomous waypoint tests, an off the shelf GPS and IMU unit were used. Based on these sensors, the current heading and location was able to be obtained. Whenever the next waypoint was input into the system, a desired heading was calculated. The error between this desired heading and current heading, as well as the distance between the current location and next waypoint was used with a PID controller to execute the desired commands. An example of this navigation is shown in Figure 35. A final GPS coordinate was selected and using the GPS's current position as well as functions to calculate the distance between GPS coordinates, the Anaconda was able to move successfully to the final GPS coordinate. In the figure, the blue line represents the path taken by the Anaconda while the green point represents the starting point. The red point is the final GPS coordinate, and the red circle encompasses an area of success. Once the Anaconda reached this circle, the boat considered itself at its destination and halts.

Based on the route taken in Figure 35, Figure 36 depicts the accuracy of the Anaconda tracking compared to an ideal path of travel for a straight line. As can be seen, the similarity between the tracking and ideal route is very close. This accuracy results in a root-

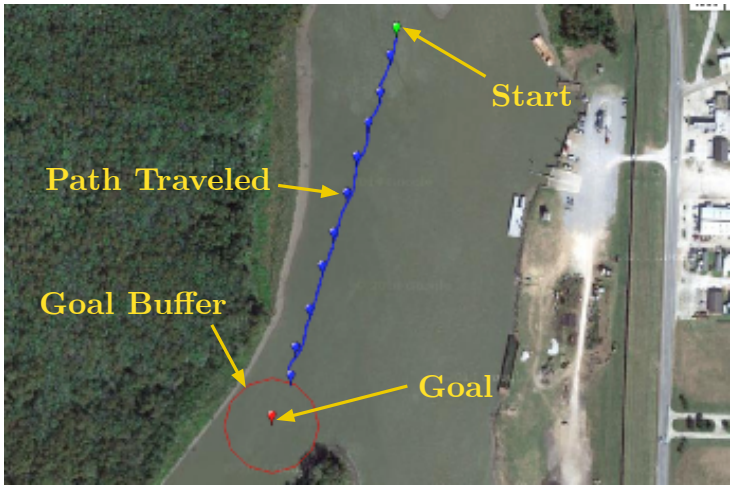

Figure 35: Path of Anaconda During Straight Line Waypoint Navigation

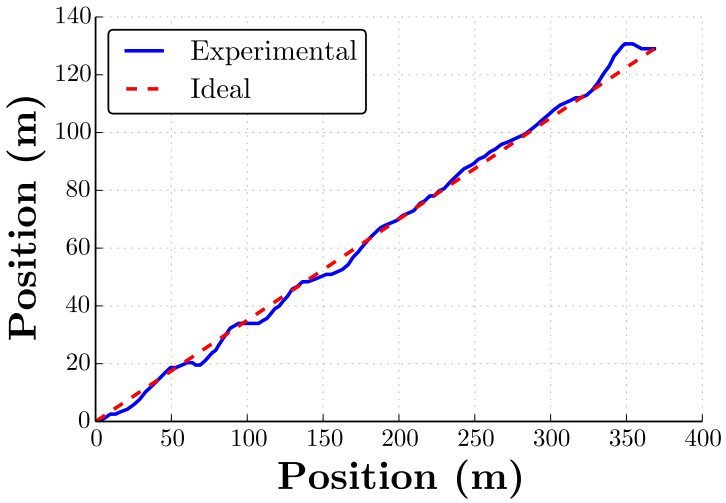

Figure 36: Comparison of Ideal and Experimental GPS Location

mean-square error of 3.2 meters which is relatively accurate, especially taking into consideration the relatively low quality sensors used.

3.2.2 Polygon Waypoint Navigation

In Figure 37, a polygon was tracked via waypoint navigation. Individual waypoints were input in the order that they needed to be reached. The green pin marks the start, and the red pin marks the ending GPS coordinate. The blue lines are the path travelled by the Anaconda with each of the waypoints marked with a blue pin. Figure 38 displays the accuracy between the path tracked and the actual path travelled. Even when traveling

through a polygon with multiple waypoints, the RMS was 6.935 meters which proves relatively accurate due to the error present in the sensors. Throughout the entire polygon, the relative accuracy of the experimental path when compared to the ideal path is very similar. Around the turns, there is more deviation from the ideal path. However, during the experiments, gains were further tuned to provide a smoother ride. The operator would not want the craft to make an abrupt turn in these cases, so the curves are rounded out to incorporate this. As seen in 38, at the beginning of the trial the Anaconda experienced drift before it began to move towards this first waypoint. If this drift is taken out then the RMS improves to 6.564 meters.

3.3 Circle and Figure 8 Waypoint Navigation

The Anaconda is also capable of tracking a circle or figure 8 pattern. This is done by selecting many waypoints along the path. The fewer waypoints that are selected the straighter the sides will be. As the amount of waypoints increases, the smoothness of the sides increases. Figure 39 represents the path taken by the Anaconda on following a circular path. As seen in the figure, with the increased number of waypoints, the blue circles that represent when the Anaconda has reached that waypoint, start to overlap. Since they overlap, the Anaconda does not have to travel to each waypoint and can therefore make smoother turns.

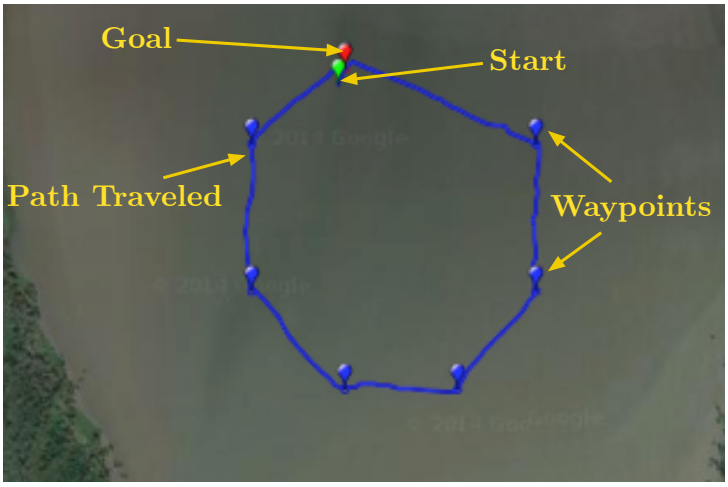

Figure 37: Path of Anaconda During Polygon Waypoint Navigation

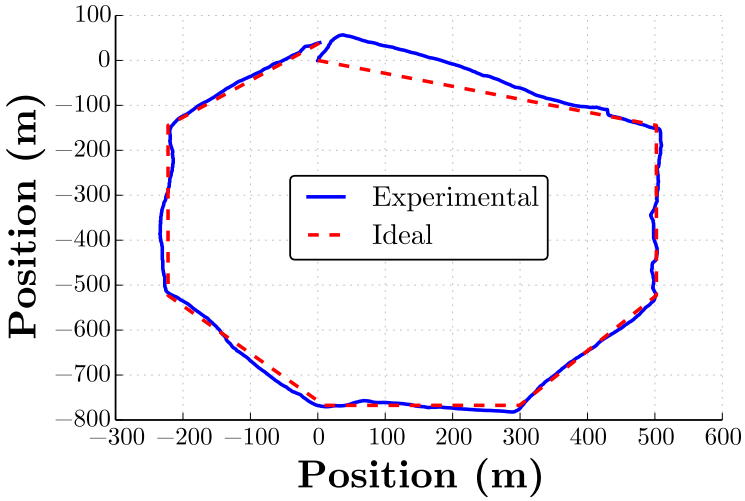

Figure 38: Comparison of Ideal and Experimental GPS Location for a Polygon

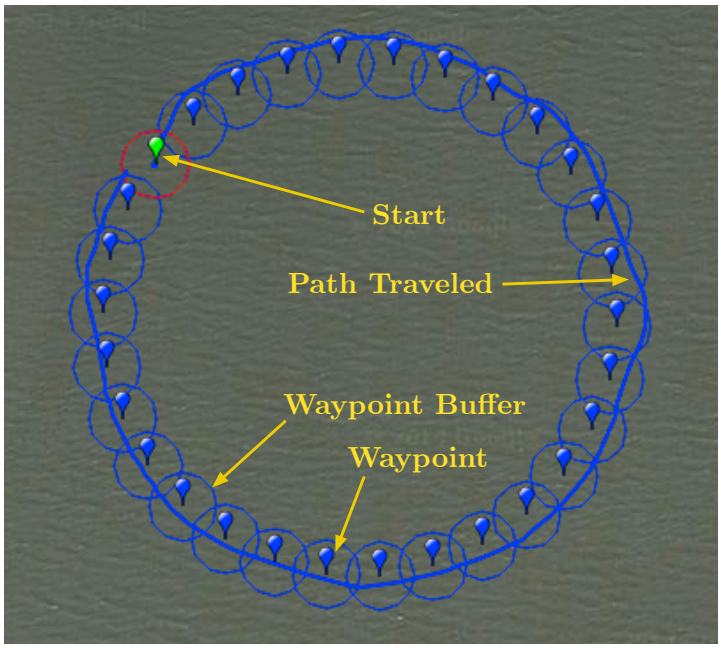

Figure 39: Path of Anaconda During Circle Waypoint Navigation

In Figure 40, the comparison between the ideal and experimental path is shown. It can be seen that the experimental path is smoother and more resembles a circle. This is due to the fact that the ideal path conducts a straight line between waypoints whereas, the Anaconda can make smoother turns once it reaches the tolerance allowed for the waypoints. There is an RMS error of 5.92 meters between the experimental and ideal path of the Ana-

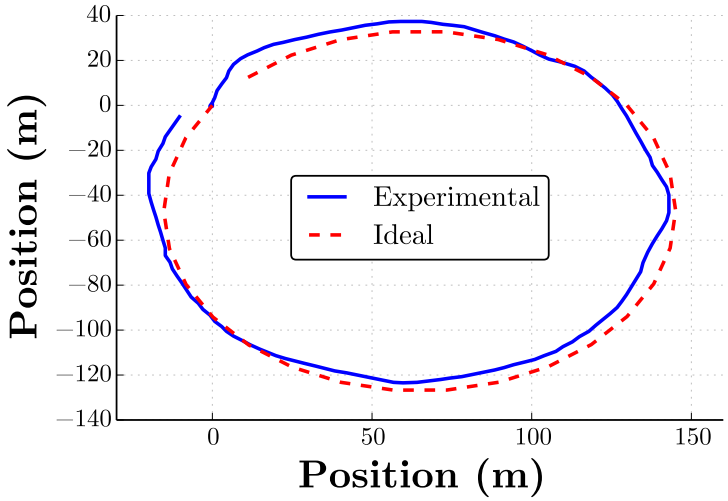

Figure 40: Comparison of Ideal and Experimental GPS Location for a Circle

conda while conducting a circular trial. Multiple experimental tests were run creating various sizes of circles. The RMS error and diameters of the circles for each of these tests is shown in Table 4. From this table, it is seen that as the circles get larger, then the RMS error also increases.

Figure 41 shows a the path of the Anaconda when conducting a figure 8 trial. The waypoints were selected in the same way of the circle, instead this time there were two circles placed together to form the figure. In the figure, the Anaconda started at the green pin and proceeded downwards in a counter-clockwise motion. As shown in Figure 39, the tolerances of the waypoints allow the Anaconda to conduct a smoother turn. Figure 42 shows the comparison between the ideal and experimental GPS data. Once again, the experimen-

Table 4: Experimental Circle Waypoints

Diameter	RMS Error
55 meters	4.02 meters
100 meters	4.63 meters
110 meters	4.97 meters
110 meters	5.07 meters
150 meters	5.78 meters
150 meters	5.84 meters
150 meters	5.83 meters
200 meters	6.04 meters

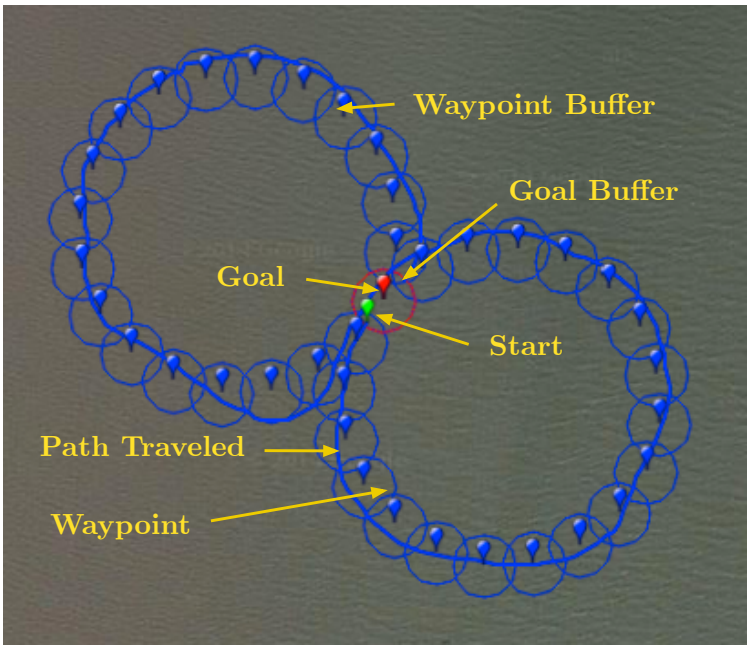

Figure 41: Path of Anaconda During Figure 8 Waypoint Navigation

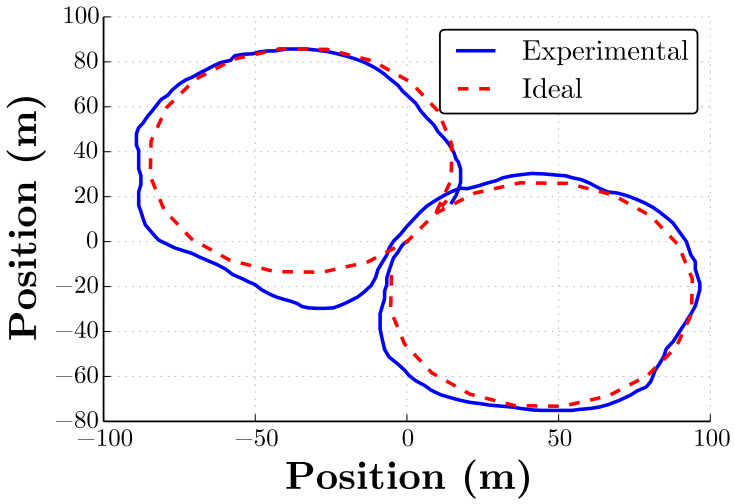

Figure 42: Comparison of Ideal and Experimental GPS Location for a Figure 8

tal data was smoother and more in line with the figure. The RMS error between these two sets of data is 5.24 meters. One other figure 8 experimental test was performed; however, this time it contained two circles with diameters of 75 meters. This figure 8 was approximately 25% smaller than the example shown in Figure 42. The RMS error between the experimental and ideal path was 4.83 meters.

3.4 Hardware and Development of a Touchscreen Controller

The electronics systems of the Anaconda utilizes the CANBus for sending and receiving signals and commands between the drive-by-wire control surfaces. Figure 43 illustrates the connectivity of the touchscreen controller to the Anaconda. In order to connect the touch-based control interface that was designed, a controls computer was connected to the existing CANBus network. A wireless local area network router was utilized to allow the wireless tablet to connect to the controls computer. The computer communicates with an onboard control unit that translates its commands into the low-level commands needs to physical control the boat, such as the buckets, nozzles, and engine throttles.

The touchscreen controller had a dead-man switch programmed into it that had to be engaged for commands to be sent. When this switch was depressed, the clutch engages and power is sent to the water jets. This wireless tablet was programmed with two control modes. Both control modes have a steering bubble, as shown in Figure 44, for control modes to be relayed to the control systems of the Anaconda. To control the throttle and steering of the boat, the operator drags the steering bubble around the device's touchscreen. The second mode of operation users the tablet's internal accelerometers and gyro-

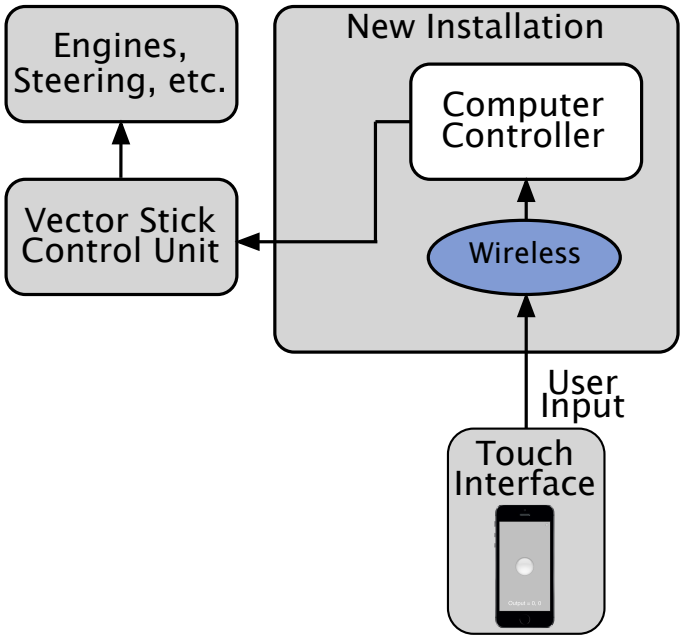

Figure 43: Diagram for the Wireless Controller Used to Steer the Anaconda

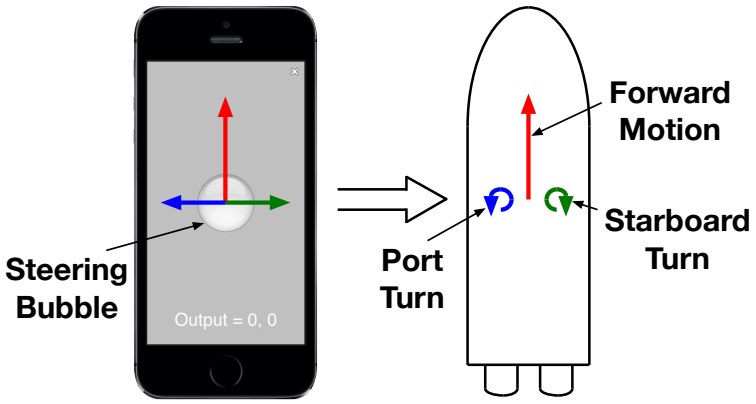

Figure 44: Touch-Based Controller Used for Boat Movements

scopes are used to allow the operator to control the boat via tilting the device. Figure 44 also shows the movements of the ship resulting from the first control mode mentioned.

4 Conclusions

This thesis presents the dynamics and the development of a model-based control for a high maneuverable marine vessel. Marine vessels are an important part of our economy as well as defense. Due to this importance and the ever increasing marine vessels on the water, there is a need for a model-based control. Model-based controls have been designed and implemented for marine vessels, however, there have been none designed for a high performance vessel such as the Anaconda. This unique application has warranted the work for this thesis. The coupling of a bucket and nozzle system makes the Anaconda have performance capabilities above most ships.

The dynamics of the Anaconda were studied and presented to provide a baseline for the model-based control. These dynamics were simplified based on assumptions that allowed forces to be combined or reduced. A simulation was created from these dynamics and proof of the accurate tracking from point-to-point was explained. To further prove the validity of the simplified model, the transfer functions that were simulated were comparable to the experimentally desired transfer functions. The uniqueness of the Anaconda was demonstrated by displaying the turning capabilities of the model using buckets compared to the nozzle steering. With these results, it is evident that the buckets are capable of performing tighter turns; however, it may not always be better to use them. It was shown that there was agreement between the model-based response and the experimental response.

Based on the system identification work and model-based control, basic autonomous navigation was achieved via GPS waypoint tracking. The accuracy of these tests was analyzed using RMS error between ideal and experimental paths between waypoints. From this thesis, a model of a highly-manueverable marine vessel was formed. A model-based controller for a highly-maneuverable marine vessel that provides basic autonomous capabilities was created along with a remote control allowing for communication between the marine vessel

and the user via a graphical user interface.

4.1 Future Work

The research in this work can be extended many ways. One interesting path is taking the model-based control and adapting it to planing speeds of the Anaconda. All of the tests in this thesis were done at non-planing speeds, allowing extensive work opportunity in higher speed capabilities. A huge path for future work is perfecting the model-based control to incorporate nozzle steering and bucket commands. Depending on the turn and speed, the control system can use a combination of both systems to provide the most effective maneuvers. This would allow the operator to maintain his attention on the helm and throttle levers instead of focusing on the bucket levers as well. This incorporation would make an extremely effective marine vessel.

Work that could also follow this model-based control would be designing a graphical user interface for operators to use. This would allow for semi-autonomous operation instead of full autonomy. However, there would always be an operator maintaining control of the marine vessel. Full autonomy of the Anaconda would be a great idea for future work. The Anaconda would have to be equipped with sensors to allow for obstacle avoidance as well as detecting shallow waterways. The on-board sensor would identify the banks of the waterway as well as any incoming vessels or stationary objects. With the performance capabilities that the Anaconda has, a marine vessel like this with complete autonomous controls would be a great asset to militaries and companies alike.

References

[1] Swiftships, *Specifications for: 35 Foot Anaconda*, Swiftships, 1105 Levee Road Morgan City, LA 70380, July 2013.

[2] D. of Defense. Predator rq-1. [Online]. Available: http://www.army-technology.com/projects/rq1-predator/rq1-predator4.html

[3] [Online]. Available: http://www.riphort.com/google-developing-autonomous-cars/

[4] [Online]. Available: http://dpmarine.dk/dynamic-positioning/

[5] Swiftships. (2014) Anaconda vessel specifications. [Online]. Available: http://www.swiftships.com/military-vessels-specifications/anaconda-socr/

[6] R. Royce. Ff-series waterjets. [Online]. Available: http://www.rolls-royce.com/marine/products/propulsors/waterjets/kamewa_ff/

[7] [Online]. Available: http://i0.wp.com/www.defensemedianetwork.com/wp-content/uploads/2014/02/AN-2.jpg

[8] R.-R. O. Ab, "Kamewa ff-series fact sheet," Rolls-Royce, P.O. Box 579 FIN-67701 Kokkola, Finland, Tech. Rep., 2002.

[9] A. Woo and D. Sprague, "Gps receivers with data ports for the uploading and downloading of absolute position information," Sep. 12 1995, uS Patent 5,450,344. [Online]. Available: http://www.google.com/patents/US5450344

[10] A. Callam, "Drone wars: armed unmanned aerial vehicles," *International Affairs Review*, vol. 18, 2014.

[11] B. V. C. G. M. S. V. Milanes, D.F. Llorca, "Clavile: Evolution of an autonomous car," in *2010 13th International IEEE Conference on Intelligent Transportation Systems (ITSC)*, 2010, pp. 1129–1134.

[12] M. Caccia, "Autonomous surface craft: Prototypes and basic research issues," in *14th Mediterranean Conference of Control and Automation*, 2006, pp. 1–6.

[13] J. E. Manley, "Unmanned surface vehicles, 15 years of development," in *Proceedings of OCEANS IEEE*, 2008, pp. 1–4.

[14] T. W. Vaneck, "Fuzzy guidance controller for an autonomous boat," *IEEE Control Systems*, vol. 17, no. 2, pp. 43–51, 1997.

[15] M. Bibuli, M. Caccia, L. Lapierre, and G. Bruzzone, "Guidance of unmanned surface vehicles: Experiments in vehicle following," *Robotics Automation Magazine*, vol. 19, 2012.

[16] Z. Yu, "Robust path following control on an unmanned boat," in *11th International Conference on Control Automation Robotics Vision*, 2010, pp. 2345–2348.

[17] *Unmanned System Integrated Roadmap.* United States Department of Defense, 2013, no. FY2013-2038.

[18] M. R. Benjamin, J. A. Curcio, J. J. Leonard, and P. Newman, "Navigation of unmanned marine vehicles in accordance with the rules of the road," in *Proceedings of IEEE International Conference of Robotics and Automation*, 2006, pp. 3581–3587.

[19] M. R. Benjamin and J. A. Curcio, "Colregs-based navigation of autonomous marine vehicles," in *Proceedings of Autonomous Underwater Vehicles*, June 2004, pp. 32–39.

[20] J. A. Curcio, J. J. Leonard, and A. Patrikalakis, "Scout - a low cost autonomous surface platform for research in cooperative autonomy," in *Proceedings of OCEANS MTS/IEEE*, 2005, pp. 725–729.

[21] J. G. N.E. Leonard, "Model-based feedback control of autonomous underwater gliders," *IEEEE Journal of Oceanic Engineering*, vol. 26, no. 4, pp. 633–645, October 2001.

[22] N. C. N. Khaled, "A dynamic model and a robust controller fora fully-actuated marine surface vessel," *Journal of Vibration and Control*, vol. 17, no. 6, pp. 801–812, n.d.

[23] M. Breivik, V. E. Hovstein, and T. I. Fossen, "Straight-line target tracking for unmanned surface vehicles," *Modeling, Identification and Control*, vol. 29, no. 4, pp. 131–149, 2008.

[24] Rafael. Rafael protector. [Online]. Available: http://www.rafael.co.il/Marketing/288-1037-en/Marketing.aspx

[25] J. Larson, M. Bruch, and J. Ebken, "Autonomous navigation and obstacle avoidance for unmanned surface vehicles," in *Defense and Security Symposium*. International Society of Optics and Photonics, 2006, pp. 623 007–623 007.

[26] F. Jenne, "Simulation control optimization of an autonomous sail boat," Master's thesis, Swiss Federal Institute of Technology Zurich, 2010.

[27] K. N. Xinping Bao, Zhenyu Yu, "Rudder based roll control via host-computer of a robotic boat," *International Journal of Advanced Robotic Systems*, vol. 6, no. 1, p. 6773, 2009.

[28] *A Comprehensive Study of Control Design for an Autonomous Helicopter*, vol. 4, December 1998.

[29] *Model-Based Executive Control Through Reactive Planning for Autonomous Rovers*, vol. 1, October 2004.

[30] T. F. M. Breivik, "Path following for marine surface vessels," in *Oceans '04. MTTS/IEEE Techno-Ocean '04*, vol. 4, November 2004, pp. 2282–2289.

[31] E. M. S. S. Jens G. Balchen, Nils A. Jenssen, "A dynamic positioning system based on kalman filtering and optimal control," *Modeling, Identification and Control*, vol. 1, no. 3, pp. 135–163, 1980.

[32] A. Sørensen, S. Sagatun, and T. Fossen, "Design of a dynamic positioning system using model-based control," *Control Engineering Practice*, vol. 4, no. 3, pp. 359–368, 1996.

[33] E. Tannuri and C. Pesce, "Comparing two different control algorithms applied to dynamic positioning of a pipeline launching barge," *Proceedings of the 10th Mediterranean Conference on Control and Automation. Lisbon, Portugal*, 2002.

[34] T. I. Fossen, "A nonlinear unified state-space model for ship maneuvering and control in a seaway," *International Journal of Bifurcation Chaos in Applied Sciences Engineering*, vol. 15, no. 9, p. 2717, 2005.

[35] T. Fossen, *Guidance and Control of Ocean Vehicles*. John Wiley Sons, 1994.

[36] G. S. A. Dhariwal, "Experiments in robotic boat localization," in *IEEE/RSJ International Conference on Intelligent Robots and Systems, 2007*, October 2007, pp. 1702–1708.

[37] T. I. Fossen, *Marine control systems: guidance, navigation and control of ships, rigs and underwater vehicles*. Marine Cybernetics AS, 2002.

[38] J. Balchen, N. Jenssen, E. Mathisen, and S. Saelid, "Dynamic positioning of floating vessles based on kalman filtering and optimal control," in *Decision and Control including the Symposium on Adaptive Processes, 1980 19th IEEE Conference on*, Dec 1980, pp. 852–864.

[39] (2014). [Online]. Available: http://global.yamaha-motor.com/business/outboards/life/boating/chapter5/

[40] K. Nomoto, T. Taguchi, K. Honda, and S. Hirano, "On the steering qualities of ships," International Shipbuilding Progress, Tech. Rep. 4, 1957.

Bergeron, Nicholas P. Bachelor of Science, Mississippi State University, Spring 2012;
Master of Science, University of Louisiana at Lafayette, Fall 2014
Major: Engineering, Mechanical Engineering Option
Title of Thesis: Model-Based Control of a High Performance Marine Vessel
Thesis Director: Dr. Joshua Vaughan
Pages in Thesis: 47; Words in Abstract 209

ABSTRACT

This thesis proposes a model-based control of a high performance marine vessel. With this model-based control, comprehensive controls based on the dynamics of the marine vessel will be obtained. The dynamics of the Anaconda, a high performance marine vessel built by Swiftships, Inc., were studied, and equations of motion reflecting the dynamics of the ship were created.

Using the equations of motion, the Anaconda was modeled and multiple point-to-point maneuvers were conducted to predict the movement of the boat in a constant current environment. Transfer functions were developed from the equations of motion and compared to transfer functions obtained from a system identification test done experimentally on the Anaconda to show the validity of the model. The system identification test consisted of a turning and acceleration response.

Using the controls gained from the model-based control, simulated heading changes were compared to experimental heading changes. These same controls were used to perform autonomous waypoint testing with the Anaconda. Since the model-based control was used the Anaconda was able to follow an ideal path relatively closely. A straight line, polygon, circle, and figure 8 autonomous waypoint tracking was performed. The RMS errors were relatively low compared to the errors present in the sensors that were used in measuring the Anaconda's performance.

Biographical Sketch

Nicholas Bergeron was born in Abbeville, Louisiana in 1989 to Bradley and Laurie Bergeron. He grew up in south Louisiana in the Jeanerette area. He graduated high school from the Louisiana School for Math, Science, and the Arts located in Natchitoches, Louisiana where he obtained the Robert Alost Hall of Fame Award. Nicholas obtained his Bachelor of Science in Biological Engineering from Mississippi State University where he was the president of the rugby team for around 5 years. He then attended the University of Louisiana at Lafayette where he will be obtaining his Master of Science degree in Mechanical Engineering.